Journal of Materials Chemistry B

PAPER

View Article Online
View Journal | View Issue

Cite this: J. Mater. Chem. B, 2014, 2, 3299

2,4-Dichlorophenoxyacetic acid functionalized gold nanoparticles: synthesis, characterization and biological effects†

Jin-Liang Jia,[ab] Li Zhu,[b] Xiao-Yong Jin,[a] Jie Wang,[a] Wei Zhang,[a] Han-Xiang Wu[a] and Han-Hong Xu*[a]

Received 12th March 2014
Accepted 29th March 2014

DOI: 10.1039/c4tb00400k

www.rsc.org/MaterialsB

Understanding and visualizing the biodistribution of agricultural chemicals inside cells and living plants is very important for enhancing targeting and changing the application approaches of chemicals. Here, a novel material was synthesized through 2,4-dichlorophenoxyacetic acid functionalized small gold nanoparticles (2,4-D-MP-Au NPs). The successful modification of Au NPs (4.46 ± 0.70 nm) was ascertained by UV-vis, TEM, FTIR and XPS. TGA data revealed about 1197 molecules of 2,4-D were coupled to the surface of one Au nanoparticle, which was sufficient for bioapplications. The optical imaging of 2,4-D-MP-Au NPs inside BY-2 cells was directly examined, revealing that 2,4-D-MP-Au NPs could be internalized in BY-2 cells by the two-photo microscopy and endocytosis, as the internalization mechanism was energy dependent for 2,4-D-MP-Au NPs. Furthermore, the biodistribution of 2,4-D-MP-Au NPs in *Ricinus* cotyledons was measured, revealing that 2,4-D-MP-Au NPs could enter into mesophyll cells of *Ricinus* cotyledons; the cell recognition was enhanced after 2,4-D conjugated Au NPs. These results indicate that the conjugates have great potential for applications on bioimaging and biolabeling for agricultural chemicals in plant physiology.

Introduction

Monitoring microscopic dynamic processes by tracking technologies has been widely used for biological phenomena such as transport in cells,[1,2] intracellular localization[3] and cell recognition.[4] Conventional tracking methods, including radioisotopes,[5,6] fluorescent dyes[7,8] and quantum dots[9] have been usually used to label and visualize drugs, however, these potential applications are limited due to radioactivity risks, photobleaching, short half-life[10] and inherent toxicity.[11] Recently, a promising approach has been published that uses gold nanoparticles (Au NPs) as optical labels owing to their biocompatibility and nontoxicity.[12,13] For example, Chan *et al.* reported the intracellular uptake of different sized and shaped Au NPs, which would have implications for the chemical design of nanostructures for biomedical applications.[14] Chen *et al.*[15] investigated the influence of Au NP conjugates on their toxicity and cellular uptake, and indicated that the aspect ratio and surface coating were critical for cellular uptake. Clearly, the degree of uptake and cellular distribution of Au NPs depended upon size of nanoparticles and surface ligand.[16] In addition, cellular portals as the nuclear pore complex would only allow a maximum size of 8 nm for a substance to passively cross the nuclear membrane.[17] Furthermore, the smaller Au NPs as labels had a greater chance that their motion was unhindered. To investigate the capabilities of labeled ligands by Au NPs as active nanotools, exploiting interactions between drug-functionalized Au NPs with small size and biota are of significant interest.

Phenoxyalkanecarboxylic acids were chosen as xenobiotics owing to the variety of products available. Of these, 2,4-dichlorophenoxyacetic acid (2,4-D), a model herbicide, has been widely used in homes, gardens and agriculture.[18] Although the process in the pesticide discovery possesses a pattern similar to that in the drug discovery, the application of nanotechnology to plant systems has lagged behind.[19] To the best of our knowledge, the cellular uptake mechanism of 2,4-D through nanotechnology has not been investigated. Hence, given the shortcoming of conventional labeling for agricultural chemicals, the development of a small Au NP-based imaging agent would fulfill a significant tracked need in plant physiology.

Herein, we first report 2,4-D functionalized Au NPs with small size that acted as a marker in tobacco bright yellow 2 (BY-2) cells and *Ricinus* cotyledons. The hybrid structure of as-prepared materials was analyzed by UV-vis, FTIR, XPS and TGA.

[a]*State Key Laboratory for Conservation and Utilization of Subtropical Agro-bioresources, South China Agricultural University, Guangzhou, Guangdong 510642, China. E-mail: hhxu@scau.edu.cn; Fax: +86-20-38604926; Tel: +86-20-85285127*

[b]*Institute of Biomaterials, College of Sciences, South China Agricultural University, Guangzhou, Guangdong 510642, China*

† Electronic supplementary information (ESI) available: UV-vis spectra of MP-Au NPs and 2,4-D-MP-Au NPs (Fig. S1). XPS spectra of MP-Au NPs and 2,4-D-MP-Au NPs (Fig. S2). See DOI: 10.1039/c4tb00400k

The stable luminescence and biodistribution of 2,4-D conjugated Au NPs were investigated by two-photon microscopy and TEM technology. Moreover, we present the investigation of the cellular uptake mechanism and uptake ratio in *Ricinus* cotyledons. The utilization of the intrinsic physical properties of Au NPs has good potential for the labeling and optical imaging of agricultural chemicals in living plants.

Materials and methods

Reagents and materials

Tetrachloroauric acid ($HAuCl_4 \cdot 3H_2O$, Acros, ACS reagent), sodium borohydride ($NaBH_4$, Sigma-Aldrich, 99%), 4-mercaptophenol (MP, J&K, 99%) and *N*,*N*′-diisopropylcarbodiimide (DIPC, J&K, 99%) were used as received. The vessels and glassware used in the experiments were carefully cleaned with aqua regia (HCl–HNO_3) and rinsed with deionized (DI) water.

Synthesis of MP-Au NPs

MP-Au NPs were synthesized according to a published procedure but with some minor modification.[20] 60 mg $HAuCl_4 \cdot 3H_2O$ and 46 mg MP were added into the mixture solution of 30 mL methanol and 0.6 mL acetic acid. 6 mL fresh $NaBH_4$ (0.4 mol L^{-1}) was quickly injected into the resulting solution with vigorous stirring. After stirring for 30 min, the mixture solution was concentrated to approximately 5 mL *in vacuo* at 45 °C. The residue was diluted with 30 mL tetrahydrofuran and 60 mL methylene chloride, and the organic solvent was extracted six times by DI water. The organic layer was concentrated to dryness *in vacuo* at 45 °C. Then 20 mL methylene chloride was added and the mixture was sonicated for 30 s. Finally, 20 mL hexane was added into the above mixture to precipitate partial Au NPs. The as-prepared suspension was split into 2 vials and centrifuged for 10 min at 10 000 rpm. The supernatant was removed by decantation. A new portion of methylene chloride was added to the precipitate, and the suspension was sonicated 30 s. This centrifugation was repeated many times; the mass of the as-prepared precipitate (MP-Au NPs) was 60 mg after dryness *in vacuo* at 45 °C.

Synthesis of 2,4-D-MP-Au NPs

Firstly, 4-(*N*,*N*-dimethylamino)pyridinium-4-toluenesulfonate (DPTS) was synthesized according to procedures reported previously.[21] Secondly, 50 mg 2,4-D and 20 mg MP-Au NPs were added into 1 mL dry *N*,*N*-dimethylformamide and 4 mL dry methylene chloride in a 50 mL dry flask with stirring. 25 mg DPTS and 150 μL DIPC were added to the above suspension after stirring 2 min. The suspension was stirred overnight at room temperature. DI water was added into the reaction solution to remove DPTS and *N*,*N*-dimethylformamide, and this protocol was repeated five times using DI water of the same volume. The methylene chloride layer was concentrated to dryness. 5 mL ethanol was added into this flask, and the mixture was sonicated for 30 s. Finally, the turbid liquid was centrifugated at 6000 rpm for 10 min, and the colorless solution was decanted. This centrifugation was repeated three times by added ethanol. The residual solvents were removed under vacuum at 45 °C; at that point the mass of the black solid was 24.3 mg.

Cellular incubation with 2,4-D-MP-Au NPs

The BY-2 cells were cultured in Murashige–Skoog medium as described by Kumagai-Sano *et al.*[22] In brief, the BY-2 cells were grown in 30 mL of culture medium (pH 5.8) containing 0.05% Tween 20 for 5 days with continuous agitation (130 rpm, 27 °C, dark). Then cell samples were obtained from 5-day-old cultures during the rapid growth phase.

For quantifying conjugation into BY-2 cells, 5-d-old cultured cells were transferred to fresh medium for 30 min at 27 °C. The dimethyl sulfoxide (DMSO) solution of 2,4-D-MP-Au NPs was diluted by the culture medium and incubated with BY-2 cells for 2 h at 27 °C. Cell aliquots were taken at the indicated times, centrifuged at 2000 rpm for 5 min, and the supernatant was discarded. Then the pellet was washed with 1 mL medium. To remove all unabsorbed 2,4-D-MP-Au NPs, the centrifugation steps and the washing procedure were repeated three times. After the final washing, the cells were resuspended in 1 mL water, sonicated for 30 s and centrifuged at 13 000 rpm for 10 min. For dry weight measurement, 30 mL aliquots were harvested on filter paper, dried together with the filter paper at 80 °C for 24 h, followed by the quantitative analysis of Au content by inductively coupled plasma optical emission spectroscopy (ICP-OES).

Endocytosis mechanism investigation: low temperature incubation at 4 °C: cellular incubations were carried out as described above with the solution kept at 4 °C, instead of the usual 27 °C condition.

Incubation of cells in 2,4-D-MP-Au NPs under adenosine triphosphate (ATP) depletion: the BY-2 cells were preincubated in media supplemented with 10 mM NaN_3 at 27 °C, followed by incubation with 2,4-D-MP-Au NPs for 2 h.

Uptake in cotyledon discs

This procedure was carried out as reported previously.[23] Briefly, cotyledon discs were made using a 12 mm diameter cork borer from *Ricinus* cotyledons. This discs were floated on preincubation medium containing 20 mM MES as buffer (pH 6.0), 250 mM mannitol, 0.25 mM $MgCl_2$, 0.5 mM $CaCl_2$ and 0.05% Tween 20. After a 30-min preincubation period, the discs were incubated in 4 mL medium containing 5.583 μg mL^{-1} 2,4-D-MP-Au NPs and 13.852 μg mL^{-1} MP-Au NPs, respectively. Then these discs were gently oscillated on a reciprocal shaker at 100 rpm and 27 °C. At the end of incubation, the 12 discs were rinsed (three times for 2 min each) in a solution of pure water–acetone (9/1, v/v), ensuring that all Au NPs on the cotyledon surface were washed away. The discs (12 discs for each treatment) were digested using a mixture 12 mL of HNO_3 and 6 mL of $HClO_4$ on a hot plate (~100 °C) and analyzed for Au content by ICP-OES.

Analysis and characterization methods

UV-vis spectra were recorded on a Unico UV-2102PC spectrometer operated at a resolution of 0.5 nm using a quartz cell with a 1 cm light-path. Fourier transform infrared transmission spectroscopy (FTIR) was recorded using a PE 2000 FTIR spectrometer and KBr as a standard for back-ground correction.

Transmission electron microscopy (TEM) images were performed on a JEOL JEM-2010 microscope operated at 120 kV. Additionally, leaf sections were analyzed by TEM technology using well-established protocols.[24] X-ray photoelectron spectroscopy (XPS) measurements were carried out on a PHI 5300 ESCA1610 SAM instrument equipped with Mg Kα radiation. Thermogravimetric analysis (TGA) of the sample was performed on a Mettler Toledo DTA/SDTA851 instrument with a heating rate of 10 °C min^{-1} under nitrogen at a flow rate of 40 mL min^{-1}.

The cells were covered with a coverslip to obtain the confocal images. The 800 nm light from a Ti:sapphire laser (Mira 900, Coherent) with a duration of 130 fs and a repetition of 76 MHz was introduced into an inverted microscope (Axio Observer A1, Zeiss). Two-photon luminescence (TPL) emitted from Au NPs was collected by the same objective lens and analyzed in a spectrometer (SR-500i-B1, Andor) with a charge-coupled device.

Results and discussion

UV-vis

Fig. S1 (ESI†) shows UV-vis spectra of chloroform solutions of MP- and 2,4-D-protected Au NPs. No localized surface plasmon resonance (LSPR) peak of MP-Au NPs can be detected around 520 nm, which confirms that the size of Au NPs is below the critical size of ~3 nm.[25] The LSPR peak of 2,4-D-MP-Au NPs is not apparent. Additionally, the spectra also show a peak of around 210 nm should be assigned to MP molecule;[20] however, a characteristic absorption peak about 290 nm originates from the 2,4-D ligands.[26] Therefore, the results prove that the 2,4-D is successfully conjugated with MP-Au NPs.

TEM

As shown in Fig. 1(a), the average dimension of MP-protected Au NPs is 2.67 ± 0.38 nm by analysis of at least 260 Au NPs. However, the average dimension of 2,4-D-MP-Au NPs is 4.46 ± 0.70 nm. It is obvious that the dimensions of Au NPs have changed after conjugation of the 2,4-D with MP-Au NPs. This phenomenon is in disagreement with one of the previous studies.[27] The effect may be attributable to the Oswald ripening process.[28] In this process, tiny Au NPs with each other in solution can form larger nanoparticles. The Au NPs with small dimensions in the *N*,*N*-dimethylformamide are more easily dissolved and redeposit onto the surface of larger Au NPs. In addition, the measured interparticle distance is 24.0 Å determined by analyzing Au NPs as shown in Fig. 1(b), to investigate the nanoparticles' borders more precisely. The calculated length of fully extended 2,4-D molecular and MP is ~14.58 Å (ref. 29–31) and 8 Å,[32] respectively. The van der Waals radial diameter of the as-prepared ligand after esterification is about

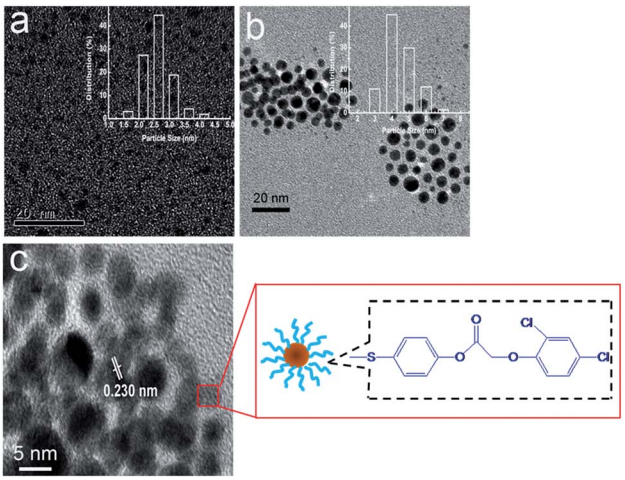

Fig. 1 TEM images of (a) MP-Au NPs and (b) 2,4-D-MP-Au NPs; (c) scheme of structure and HRTEM images of 2,4-D-MP-Au NPs.

22.58 Å. Comparison of the estimated ligand length and the experimental results (~24.0 Å) by analyzing Au NPs in Fig. 1(b) shows that the interparticle distance is slightly larger than the length of a fully extended ligand. However, the interparticle distance is not the sum of two fully extended ligand lengths (~45.2 Å). This indicates that the organic ligands on Au NPs surface are interdigitated and that the particle-to-particle distances are decreased, which is in agreement with the results of alkane chains protecting Au NPs.[33]

HRTEM images of 2,4-D-MP-Au NPs are shown in Fig. 1(c). The majority of particles exhibit the characteristic lattice fringes that represent the individual atomic layers. The *d*-spacing between the fringes is 0.204 and 0.235 nm, which corresponds to the {200} and {111} crystallographic planes of fcc Au. The majority of particles show that the crystallographic plane in Fig. 1(c) is {111} because the calculated *d*-spacing is 0.230 nm; there is also a little occasional twinning of particles. Importantly, HRTEM images demonstrate Au NPs exist.

FTIR

To confirm that the functional ligand was successfully synthesized, these samples were characterized by FTIR spectra. Comparing Fig. 2(a) with 2(b), the IR spectra show clear evidence that MP forms part of the composite. The spectrum of MP gives a weak stretching band at 2560 cm^{-1}, which is assigned to the S–H group (curve a). However, this peak is absent in the MP-Au NPs (curve b), suggesting that the thiol hydrogen has been self-assembled as a monolayer on gold surfaces, and that there are chemical interactions between Au atom and S atom. As shown in Fig. 2(c), the peaks of 2,4-D-MP-Au NPs were carefully analyzed and the following assignment was performed:[34] the appearance of the peaks at 1163 and 1776 cm^{-1} can be attributed to ester groups, and 1776 cm^{-1} is the characteristic vibrational mode of the carbonyl group. These peaks at 1649, 1578 and 1482 cm^{-1} are assigned to the aromatic ring. There is a weak split peak at 1649 cm^{-1} because of the conjugate mode *via* the interaction between the aromatic ring and oxygen atom in the ester group. The CH

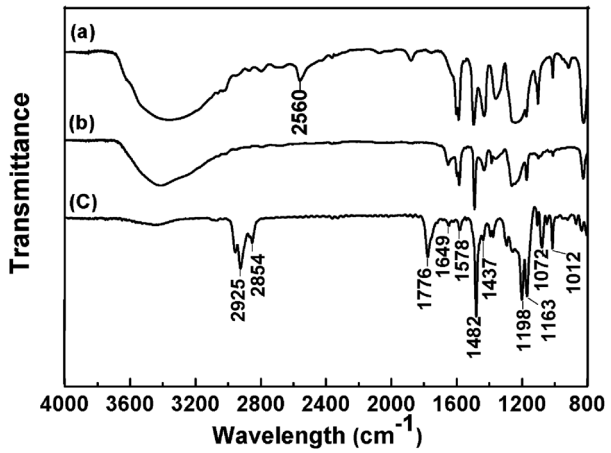

Fig. 2 FTIR spectra of (a) MP, (b) MP-Au NPs and (c) 2,4-D-MP-Au NPs.

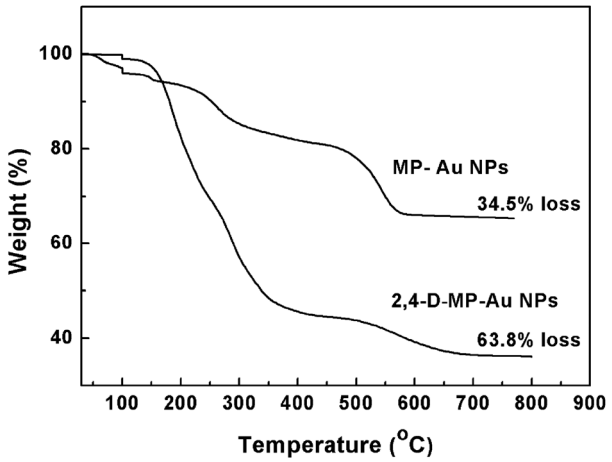

Fig. 3 TGA data measuring the loss of organic ligands corresponding to MP-Au NPs and 2,4-D-MP-Au NPs.

stretching vibration in the aromatic ring is a weak peak at 3072 cm^{-1}. Additionally, the peaks at 2925 and 2854 cm^{-1} arise from the asymmetric and symmetric stretching vibration peaks of CH_2 in the 2,4-D, and the peaks at 1198 and 1072 cm^{-1} are due to the C–O vibration in Ph–O–CH_2 groups. The peak at 1012 cm^{-1} is attributed to Ph–O, and the other peak at 1437 cm^{-1} is typical of the C–C vibration in the CH_2–C═O group. By contrast, IR spectra confirm that the reaction between 2,4-D and MP-Au NPs has occurred.

XPS

To gain further insight into the formation of the surface composition and Au atoms in samples, XPS measurements were conducted. As shown in Fig. S2a (ESI†), there were two peaks located at binding energies of 87.9 and 84.2 eV for MP-Au NPs,[35] but that they differed from the value for 2,4-D-MP-Au NPs. This indicates interaction between 2,4-D and MP-Au NPs. In Fig. S2b (ESI†), a photoelectron peak with binding energy 163.3 eV is assigned to the orbital doublet arising from S 2p1/2.[32] Moreover, there is no peak at 164 eV in Fig. S2b (ESI†), which would be assigned to the thiol binding energy of MP;[36] this indicates MP has conjugated with Au NPs. This conclusion is in good agreement with the result of the FTIR. Though a peak at 168.9 eV corresponds to small amounts of oxidized sulfur species,[37] there is no oxidized sulfur species in 2,4-D-MP-Au NPs because these oxidized sulfur species on the surface of gold could be washed by centrifugation. Additionally, the detectable Cl 2p peaks are attributed to the 2,4-D-MP-Au NPs in Fig. S2c (ESI†), thereby suggesting the successful formation of 2,4-D-MP-Au NPs.

TGA

To corroborate the number of MP and 2,4-D molecules attached to each Au particle, MP-Au NPs and 2,4-D-MP-Au NPs were analyzed using TGA data (Fig. 3). The average size of MP-Au NPs is calculated to be 2.67 ± 0.38 nm by TEM; thus the volume per nanoparticle is approximately 9.96 nm^3 based on its sphere. So approximating the amount of Au atoms per nanoparticle is then $4 \times 9.96/0.0679 = 587$ ($M_{Au} = 115\,639$ Da) using the fcc unit cell volume, and the amount of organic ligands (MP) is approximately 487 per particle due to the organic content (34.5 wt%) in nanoparticles. The MP number of unit volume is determined to be 49 nm^{-3}. This value is higher than has been previously reported in the literature,[27] which may result from the different size of nanoparticles. Additionally, the mass of dried 2,4-D-MP-Au NPs could become 24.3 mg owing to the esterification using 20 mg MP-Au NPs and excess 2,4-D. Hence, the mass percent of conjugated 2,4-D with MP-Au NPs is 17.7% and the molecular weight of 2,4-D-MP-Au NPs is then 538 795 Da. The number of 2,4-D conjugated MP-Au NPs approaches 1197 according to the organic content (63.8%) of 2,4-D-MP-Au NPs with 4.46 ± 0.70 nm. Therefore, this is a very good method for evaluating organic core–shell nanostructure.

Cell imaging and uptake

The TPL from the Au NPs was determined to monitor the distribution of 2,4-D-MP-Au NPs entering into the BY-2 cells. As shown in Fig. 4, TPL spectra were recorded in the time-course experiments after the switching-on of the laser light with an excitation wavelength of 800 nm. TPL images from at least three randomly selected sites of BY-2 cells were acquired under identical experimental conditions. The detector positions were highlighted by red circles. In a control experiment (Fig. 4(a) and (d)), no TPL signal was observed in various sites, including the extracellular environment, cytoplasm and nucleus. However, in Fig. 4(b), (c), (e) and (f), the bright dots of different sites inside the cells can be detected, which affirms that Au NPs can emit strong TPL when the fs laser wavelength is in resonance with their longitudinal surface plasmon resonance (LSPR).[38] Moreover, TPL can be distinguished from the autofluorescence of plant tissues using an excitation wavelength of 800 nm, which agrees well with values reported in the literature.[39] Because TPL can be used as a reliable tool for quantitative imaging of Au NPs,[40] we investigated the TPL intensity from 2,4-D-MP-Au NPs in the cytoplasm and nucleus of BY-2 cells. Insets show that the

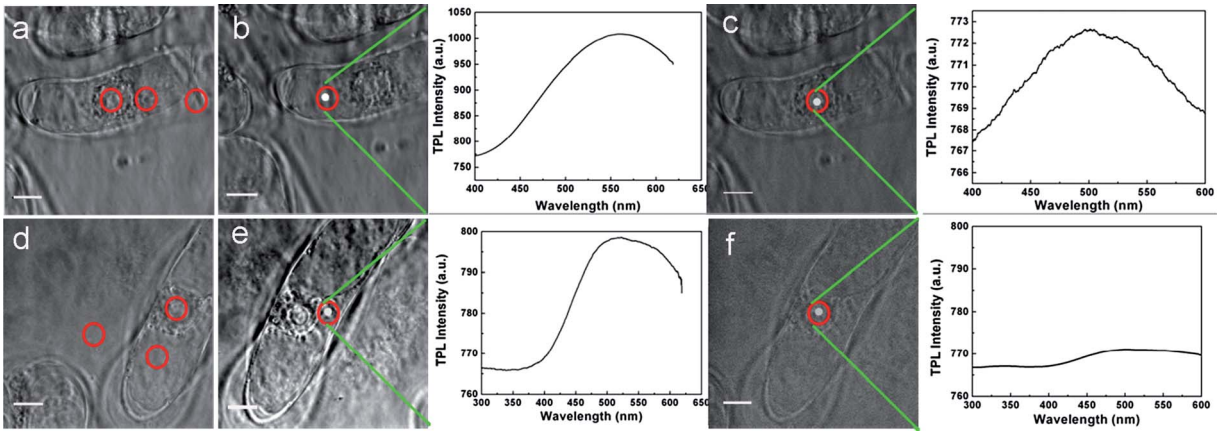

Fig. 4 TPL images of BY-2 cells: (a and d) control experiments after 12 and 24 h, respectively; (b and c) treatment with 80 μg mL^{-1} 2,4-D-MP-Au NPs for 12 h; (e and f) treatment with 80 μg mL^{-1} 2,4-D-MP-Au NPs for 24 h. For clarity, TPL positions are highlighted by red circles. Insets: the graphs of fluorescence intensity in the cytoplasm and nucleus of the BY-2 cells.

TPL intensity weakens gradually with time. However, almost no Au NPs could be detected in the nucleus at 24 h. Taken together, the TPL intensity inside BY-2 cells decreases from 12 to 24 h, suggesting that 2,4-D-MP-Au NPs have be internalized and excluded with passage of time.

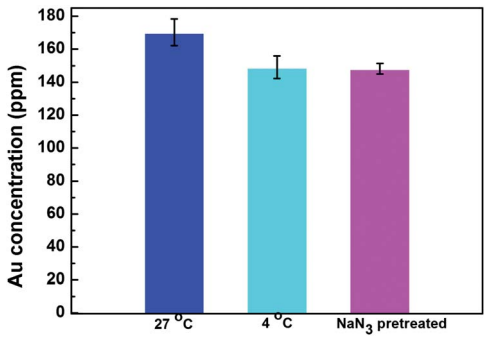

Fig. 5 Cellular uptake of BY-2 cells for 2,4-D-MP-Au NPs under different conditions. The cellular uptake was inhibited both at 4 °C and in the presence of NaN_3 ($n = 3$, ±SE).

In this study, Au NPs can also be quantified in BY-2 cells using the techniques of ICP-OES. The investigation of the cellular internalization mechanism and pathway for Au NPs-coated with 2,4-D molecular will provide important information for the advancement of Au NPs for applications to delivery and labeling of chemicals. In the present experiments, the 2,4-D-MP-Au NPs were incubated with the BY-2 cells at low temperature (4 °C instead of 27 °C) or in ATP-depleted environments (cells pretreated with NaN_3). As we know, endocytosis was known as a general entry mechanism for various extracellular materials and was an energy-dependent uptake.[41,42] Indeed, a decrease in the uptake of the 2,4-D-MP-Au NPs can be observed after incubation at 4 °C or ATP depletion by NaN_3 (Fig. 5), suggesting that the internalization of 2,4-D-MP-Au NPs is energy dependent. Thus, the receptor-mediated endocytosis is the predominant mechanism for 2,4-D-MP-Au NPs in BY-2 cells.

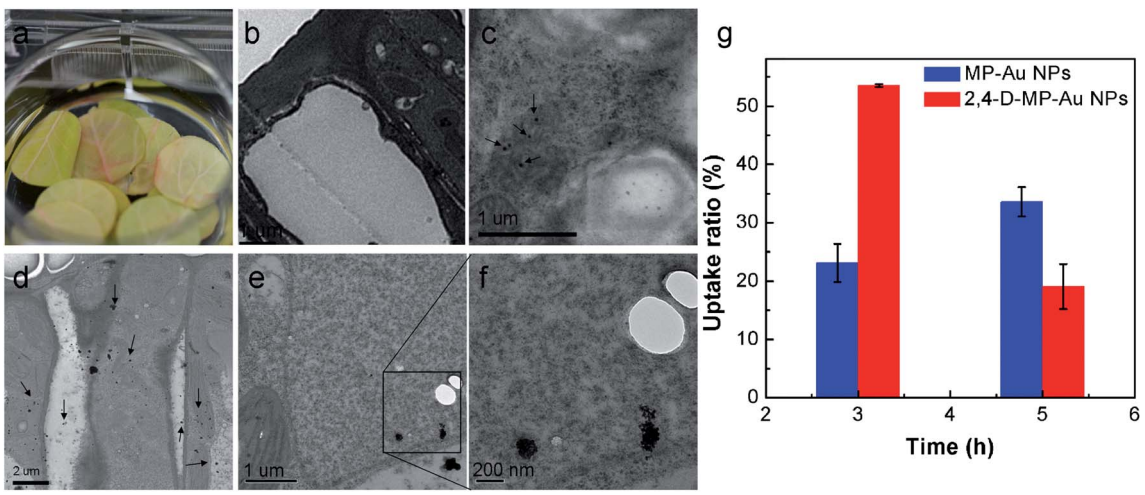

Fig. 6 (a) Photographs of *Ricinus* cotyledons. Typical TEM images of a mesophyll cell: (b) a control experiment; (c) treatment with MP-Au NPs for 5 h; (d and e) treatment with 2,4-D-MP-Au NPs for 5 h; (f) representative high-magnification TEM image of the square part in (e) photograph; (g) uptake ratios of MP-Au NPs and 2,4-D-MP-Au NPs ($n = 3$, ±SE).

In vivo evaluation

To determine whether these Au NPs could enter into living plants, we firstly incubated MP-Au NPs and 2,4-D-MP-Au NPs in cotyledons discs. After 5 h of incubation with *Ricinus* cotyledons, MP-Au NPs and 2,4-D-MP-Au NPs were observed as dark spots in mesophyll cells by ultrathin slicing and TEM technology (Fig. 6(c) and (d), arrows). In addition, Fig. 6(e) shows that a small amount of 2,4-D-MP-Au NPs appears to be aggregated inside mesophyll cells. The results indicate that the particles can cross the plant wall and cell membrane barriers, and accumulate within the individual plant cell. Additionally, the uptake ratios of Au NPs for 12 cotyledon discs were quantitatively analyzed by ICP-OES at different times. As shown in Fig. 6(g), the uptake ratio of MP-Au NPs was 23.2% and 33.8% at 3 and 5 h, respectively, for 12 cotyledon discs. However, the uptake ratio of 2,4-D-MP-Au NPs had reached 53.5% at 3 h and then decreased to 19.1% at 5 h under identical experimental conditions, suggesting that 2,4-D-MP-Au NPs had been internalized and excluded by the *Ricinus* cotyledons over time. This conclusion is in agreement with the results of BY-2 cells. Time-course experiments show that the uptake ratio of 2,4-D-MP-Au NPs is approximately 2-fold and 0.5-fold that of MP-Au NPs at 3 and 5 h, respectively, indicating that transport and exclusion are more readily manifested after 2,4-D conjugated MP-Au NPs. This result suggests that 2,4-D molecule might enhance cell recognition.

Conclusions

In summary, small Au NPs were successfully designed by conjugating 2,4-D *via* esterification and were used in labeling a herbicide. The 2,4-D-MP-Au NPs exhibit a higher drug-loading ability, which is shown by the BY-2 cellular uptake mechanism and uptake ratio in *Ricinus* cotyledons. The results indicate that the internalization of 2,4-D-MP-Au NPs is energy dependent and the transport is more obvious after 2,4-D is conjugated with Au NPs. Moreover, the 2,4-D molecule can enhance cell recognition. These results indicate that the Au NP conjugates may be good candidates in plant physiology for future imaging.

Acknowledgements

We thank Professor Bo-Qing Xu (Department of Chemistry, Tsinghua University, China) for his kind help in discussion on measurements of TGA and XPS. This work was financially supported by NSF (Grant 31171886) of China, the Doctoral Fund of Ministry of Education of China (Grant 20114404110020 and 20134404130003).

Notes and references

1 L. Wang, Y. Liu, W. Li, X. Jiang, Y. Ji, X. Wu, L. Xu, Y. Qiu, K. Zhao, T. Wei, Y. Li, Y. Zhao and C. Chen, *Nano Lett.*, 2011, **11**, 772–780.
2 D. Stanicki, S. Boutry, S. Laurent, L. Wacheul, E. Nicolas, D. Crombez, L. V. Elst, D. L. J. Lafontaine and R. N. Muller, *J. Mater. Chem. B*, 2014, **2**, 387–397.
3 P. Nativo, I. A. Prior and M. Brust, *ACS Nano*, 2008, **2**, 1639–1644.
4 X. Li, H. Zhou, L. Yang, G. Du, A. S. Pai-Panandiker, X. Huang and B. Yan, *Biomaterials*, 2011, **32**, 2540–2545.
5 H. Alsayeda, S. Pascal-Lorber, C. Nallanthigal, L. Debrauwer and F. Laurent, *Environ. Chem. Lett.*, 2008, **6**, 229–234.
6 A. Aajoud, M. Raveton, H. Aouadi, M. Tissut and P. Ravanel, *J. Agric. Food Chem.*, 2006, **54**, 5055–5060.
7 A. L. Hu, W. Yang and H. H. Xu, *J. Photochem. Photobiol., B*, 2010, **101**, 215–223.
8 W. Yang, H. X. Wu, H. H. Xu, A. L. Hu and M. L. Lu, *J. Agric. Food Chem.*, 2011, **59**, 12534–12542.
9 A. Bhirde, J. Xie, M. Swierczewska and X. Chen, *Nanoscale*, 2011, **3**, 142–153.
10 A. Taylor, K. M. Wilson, P. Murray, D. G. Fernig and R. Levy, *Chem. Soc. Rev.*, 2012, **41**, 2707–2717.
11 X. Huang, P. K. Jain, I. H. El-Sayed and M. A. El-Sayed, *Nanomedicine*, 2007, **2**, 681–693.
12 C. M. Cobley, J. Chen, E. C. Cho, L. V. Wang and Y. Xia, *Chem. Soc. Rev.*, 2011, **40**, 44–56.
13 R. Venkatesan, A. Pichaimani, K. Hari, P. K. Balasubramanian, J. Kulandaivel and K. Premkumar, *J. Mater. Chem. B*, 2013, **1**, 1010–1018.
14 B. D. Chithrani, A. A. Ghazani and W. C. W. Chan, *Nano Lett.*, 2006, **6**, 662–668.
15 Y. Qiu, Y. Liu, L. Wang, L. Xu, R. Bai, Y. Ji, X. Wu, Y. Zhao, Y. Li and C. Chen, *Biomaterials*, 2010, **31**, 7606–7619.
16 N. B. Shah, J. Dong and J. C. Bischof, *Mol. Pharmaceutics*, 2011, **8**, 176–184.
17 G. M. Cooper and R. E. Hausman, *The Cell: a Molecular Approach*, Sinauer Associates Inc., ASM Press, WA, 2008, p. 361.
18 D. H. Garabrant and M. A. Philbert, *Crit. Rev. Toxicol.*, 2002, **32**, 233–257.
19 J. Koelmel, T. Leland, H. Wang, D. Amarasiriwardena and B. Xing, *Environ. Pollut.*, 2013, **174**, 222–228.
20 E. R. Zubarev, J. Xu, A. Sayyad and J. D. Gibson, *J. Am. Chem. Soc.*, 2006, **128**, 4958–4959.
21 J. S. Moore and S. I. Stupp, *Macromolecules*, 1990, **23**, 65–70.
22 F. Kumagai-Sano, T. Hayashi, T. Sano and S. Hasezawa, *Nat. Protoc.*, 2007, **1**, 2621–2627.
23 H. X. Wu, W. Yang, Z. X. Zhang, T. Huang, G. K. Yao and H. H. Xu, *J. Agric. Food Chem.*, 2012, **60**, 6088–6094.
24 Z. Zhang, Q. Fang, Y. He, Y. Li, H. Lu and X. Zhang, *J. Yunnan Univ., Nat. Sci. Ed.*, 1995, **17**, 82–85.
25 H. Chen, B. Li, C. Wang, X. Zhang, Z. Cheng, X. Dai, R. Zhu and Y. Gu, *Nanotechnology*, 2013, **24**, 055704.
26 R. Yu, H. Shi, M. He, J. Guo and Y. Qian, *China Environ. Sci.*, 2005, **25**, 288–292.
27 J. D. Gibson, B. P. Khanal and E. R. Zubarev, *J. Am. Chem. Soc.*, 2007, **129**, 11653–11661.
28 T. K. N. Hoang, L. Deriemaeker, V. B. La and R. Finsy, *Langmuir*, 2004, **20**, 8966–8969.

29 M. S. Chen, A. K. Santra and D. W. Goodman, *J. Phys. Chem. B*, 2004, **108**, 17940–17945.
30 J. Peller, O. Wiest and P. V. Kamat, *J. Phys. Chem. A*, 2004, **108**, 10925–10933.
31 R. E. Jones and D. H. Templeton, *Acta Crystallogr.*, 1958, **11**, 484–487.
32 D. Barriet, C. M. Yam, O. E. Shmakova, A. C. Jamison and T. R. Lee, *Langmuir*, 2007, **23**, 8866–8875.
33 D. Baranov and E. N. Kadnikova, *J. Mater. Chem.*, 2011, **21**, 6152–6157.
34 I. E. Dell'Erba, C. E. Hoppe and R. J. J. Williams, *Langmuir*, 2010, **26**, 2042–2049.
35 T. F. Jaramillo, S. H. Baeck, B. R. Cuenya and E. W. McFarland, *J. Am. Chem. Soc.*, 2003, **125**, 7148–7149.
36 P. Urchaga, M. Weissmann, S. Baranton, T. Girardeau and C. Coutanceau, *Langmuir*, 2009, **25**, 6543–6550.
37 D. G. Castner, K. Hinds and D. W. Grainger, *Langmuir*, 1996, **12**, 5083–5086.
38 H. D. Deng, G. C. Li, Q. F. Dai, M. Ouyang, S. Lan, A. V. Gopal, V. A. Trofimov and T. M. Lysak, *Opt. Express*, 2012, **20**, 10963–10970.
39 T. Wang, J. Y. Chen, S. Zhen, P. N. Wang, C. C. Wang, W. L. Yang and Q. Peng, *J. Fluoresc.*, 2009, **19**, 615–621.
40 L. Tong, W. He, Y. Zhang, W. Zheng and J. X. Cheng, *Langmuir*, 2009, **25**, 12454–12459.
41 N. W. S. Kam, Z. Liu and H. Dai, *Angew. Chem., Int. Ed.*, 2006, **45**, 577–581.
42 B. D. Chithrani and W. C. W. Chan, *Nano Lett.*, 2007, **7**, 1542–1550.